

# Phase Frustration-Induced Spatial Lattice Symmetry in the Vicsek-Kuramoto-Sakaguchi Model

Yichen Lu

August 23, 2025

## Contents

<b>1</b>	<b>The Model</b>	<b>1</b>
<b>2</b>	<b>Phase Frustration-Induced Crystallization</b>	<b>3</b>
2.1	Key properties . . . . .	3
2.1.1	Snapshots and phase diagram . . . . .	4
2.1.2	Respiration-like motion of unit cells . . . . .	10
2.1.3	Lattice constant . . . . .	12
2.1.4	Initial conditions determined cells composition . . . . .	13
<b>3</b>	<b>Critical condition for phase transition and mechanism</b>	<b>14</b>
3.1	Linear stability analysis with amplitude ansatz . . . . .	14
3.2	Abstract phase oscillator model . . . . .	15

## 1 The Model

Particles have a spatial position  $\mathbf{r}_i = (x_i, y_i)$  and an internal phase  $\theta_i$  which evolve according to equations:

$$\dot{\mathbf{r}}_i = v \mathbf{p}(\theta_i) , \quad (1a)$$

$$\dot{\theta}_i = \frac{K}{|A_i|} \sum_{j \in A_i} [\sin(\theta_j - \theta_i + \alpha) - \sin \alpha] , \quad (1b)$$

for  $i = 1, 2, \dots, N$ . Here in Eq. (1a),  $\mathbf{p}(\theta) = (\cos \theta, \sin \theta)$ , which means each particle rotates with a constant speed  $v$  in the direction of its instantaneous phase  $\theta_i(t)$ . The particles are treated as point-like with no direct spatial interactions, consistent with classical models of chiral self-propelled particles [1–3, 7, 8]. As per Eq. (1b), the mean runs over neighbors within a coupling radius  $d_0$  around particle  $i$ :

$$A_i(t) = \{j \mid |\mathbf{r}_i(t) - \mathbf{r}_j(t)| \leq d_0\} , \quad (2)$$

$K (\geq 0)$  is the coupling strength,  $\alpha$  is the phase frustration between two neighboring particles. When  $\alpha_0 = 0$ , the dynamics reduces to the normal Vicsek-like model. The introduction of counter term  $-\sin \alpha$  ensures that the interaction force cancels exactly when phase differences vanish ( $\theta_j - \theta_i = 0$ ). This guarantees that perfect synchronization is always an equilibrium state. Without this term, synchronized oscillators would experience a net force  $K \sin \alpha$ , artificially shifting their frequencies [6].

Some necessary order parameters can be introduced to measure the level of coordination among swarmalators in space motion and phase dynamics. Firstly, at the macroscopic level, the system may be described by the single-partial distribution  $\rho(\mathbf{r}, \theta, t)$ , which satisfies the normalization condition

$$\int_{L \times L} d^2 \mathbf{r} \int_0^{2\pi} d\theta \rho(\mathbf{r}, \theta, t) = 1 , \quad (3)$$

where  $L$  is the size of the system in two dimensions. Next, we define the coarse-grained spatial density  $\varrho(\mathbf{r}, t)$  and the global polarization  $p(\theta, t)$  density by integrating  $\rho(\mathbf{r}, \theta, t)$  over the phase and spatial, respectively:

$$\varrho(\mathbf{r}, t) = \int_0^{2\pi} \rho(\mathbf{r}, \theta, t) d\theta , \quad (4a)$$

$$p(\theta, t) = \int_{L \times L} \rho(\mathbf{r}, \theta, t) d\mathbf{r} . \quad (4b)$$

In the homogeneous state, these quantities take uniform values  $(\rho, \varrho, p) = (\rho_0, \varrho_0, p_0) = (1/(2\pi L^2), 1/L^2, 1/2\pi)$ .

To measure deviations from uniformity, we define the following single-particle order parameters:

$$\rho_{\text{std}}(t) = \frac{1}{1 - \rho_0} \left[ \max_{\mathbf{r} \in L \times L, \theta \in [0, 2\pi]} \rho(\mathbf{r}, \theta, t) - \rho_0 \right] , \quad (5)$$

Similarly, we can define order parameters for spatial and phase polarization densities, denoted as  $\varrho_{\text{std}}$  and  $p_{\text{std}}$ , respectively. These order parameters range from 0 to 1, reflecting the degree of spatial and phase coherence in the system. When particles are uniformly distributed in both space and phase,  $\rho, \varrho, p_{\text{std}} \approx 0$ . Conversely, if full condensation and polarization occur,  $\rho, \varrho, p_{\text{std}} \approx 1$ .

We conducted numerical simulations to investigate the performance and characteristics of our system under various conditions. For simplicity, we assume that particles are initially distributed uniformly in a two-dimensional  $L \times L$  square with periodic boundary conditions. Unless otherwise stated, all the numerical simulations of the model Eq. (1) were run on Python using Euler integration with box size of  $L = 7$ , population sizes of  $N = 2000$ , self-propulsion speed of  $v = 3$ . For the final state and phase diagram, each data point of order parameters was collected by averaging last 500 time steps of the simulation to discard the transients.

## 2 Phase Frustration-Induced Crystallization

### 2.1 Key properties

1. [Done] What does the lattice structure look like? What is the unit cell structure, and what is the spatial arrangement of the unit cells? Besides triangular, what other spatial structures exist? In which regions of frustration does it appear? (And what are the corresponding coupling conditions and natural frequency distributions?)

Lattice structure emerges when  $\alpha \in (\pi/2, \pi]$ . For  $\pi/2 < \alpha \ll \pi$ , the lattice structure exhibits a triangular arrangement (Sometimes it is a tetragonal lattice, but in most cases it is stable in a triangular lattice), where in each cell, particles are arranged in a vortex pattern independent of natural frequency (mainly determined by initial conditions). This arrangement leads to a stable and ordered configuration, where the cells maintain a fixed distance from each other and the particles rotate in a coordinated manner in the form of cycloids, which leads to respiration-like motion of the cells. While for  $\alpha = \pi$  (anti-alignment coupling), the system transforms into a double-lane structure with particles in each lane propelling in opposite directions.

2. [Done] What is each cell composed of?

Each cell is composed of particles with the neighboring particles at initial conditions, whose criterion is discussed in Sec. 2.1.4.

3. [Done] What is the internal dynamics within a cell?

Within a cell, particles are all-to-all coupled, and they rotate in a Kuramoto-like manner.

4. [Done] What determines the length (periodicity)? (Interaction distance?)

The lattice constant (distance) is determined by the coupling strength  $K$ , the radius  $d_0$ , and the frustration  $\alpha$ . For  $\alpha \gtrsim 0.5\pi$  The theoretical lattice constant is given by Eq. (7).

### 2.1.1 Snapshots and phase diagram

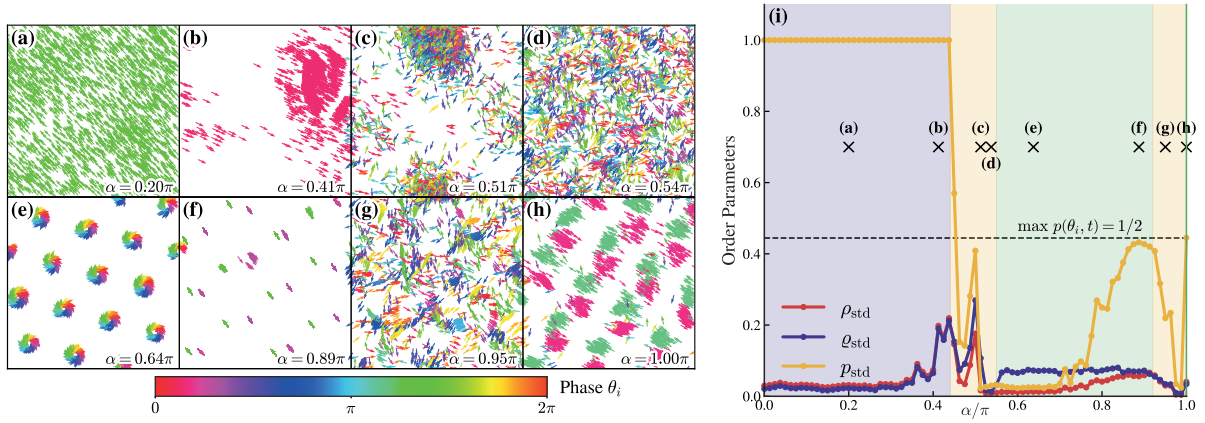


Figure 1: (a)-(h) Representative simulation snapshots for synchronization state [(a), (b)] and disordered state [(c), (d), (g)] and lattice state [(e), (f), (h)] at different phase frustration  $\alpha$ . The orientation and color of particles represent their instantaneous phase  $\theta_i$ . (i) Phase diagram and order parameters of the system with respect to the phase frustration  $\alpha$ . The crosses mark the snapshots in (a)-(h). Regions of blue, yellow and green (with single point  $\alpha/\pi = 1$ ) respectively represent the synchronized, nonuniform disordered, uniform disordered states.

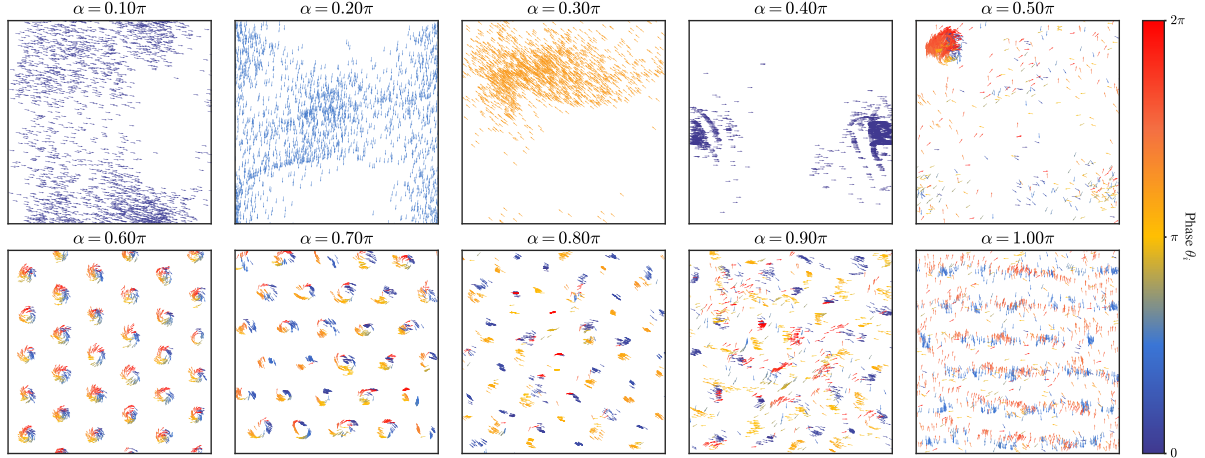


Figure 2: Snapshot of the achiral system ( $\omega_{min} = 0$ ,  $\Delta\omega = 0$ ) at  $t = 200$  with  $N = 2000$ ,  $K = 20$ , and  $d_0 = 1$ .

The phase diagram of the system is constructed by varying the key parameters, including the coupling strength  $K$ , the radius  $d_0$ . The resulting patterns are classified into ordered and lattice states.

Single chirality particles can also form a triangular lattice structure:

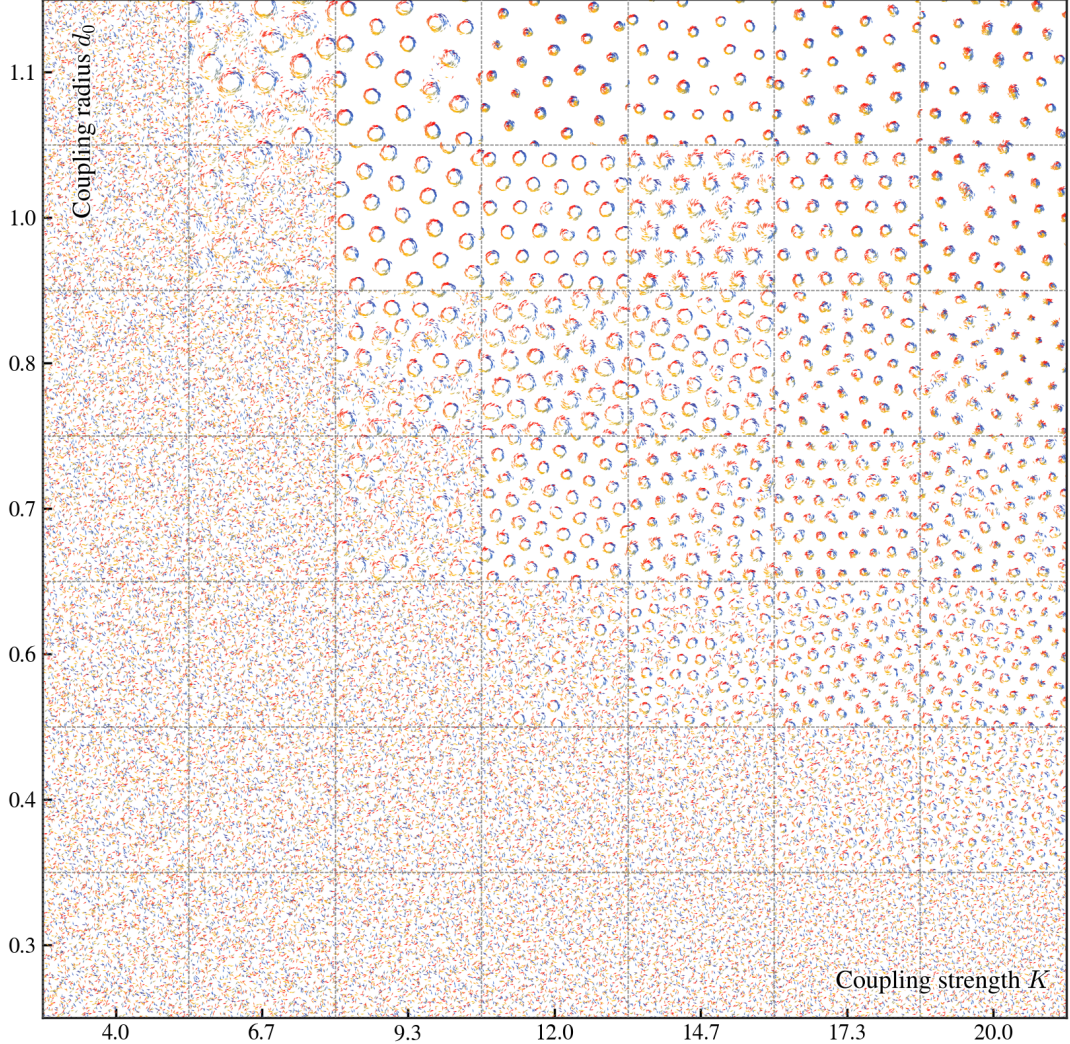


Figure 3: Snapshots of asymmetric chiral system ( $\omega_i \sim [0, 2]$ ) at different coupling strengths  $K$  and radius  $d_0$  for  $\alpha = 0.6\pi$ .

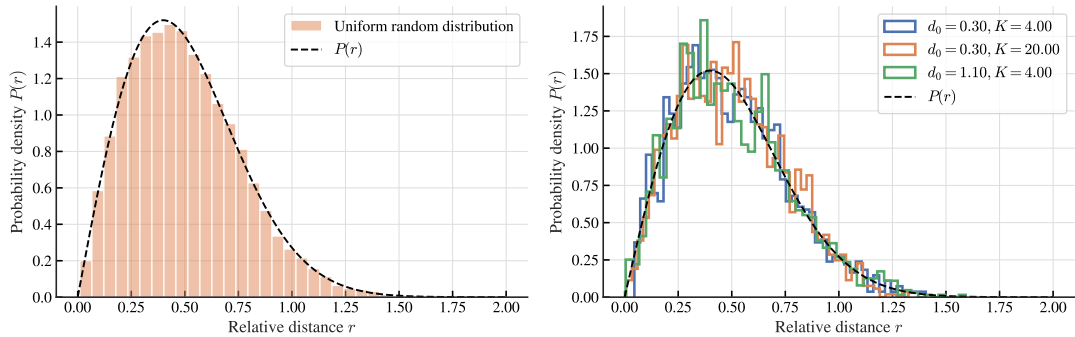


Figure 4: The probability distribution functions (PDF) of distances,  $r$ , normalized with the mean particle spacing,  $r_0$ . The dash line is the PDF of Rayleigh Distribution  $P(r) = 2\pi r \exp [-\pi r^2]$ .

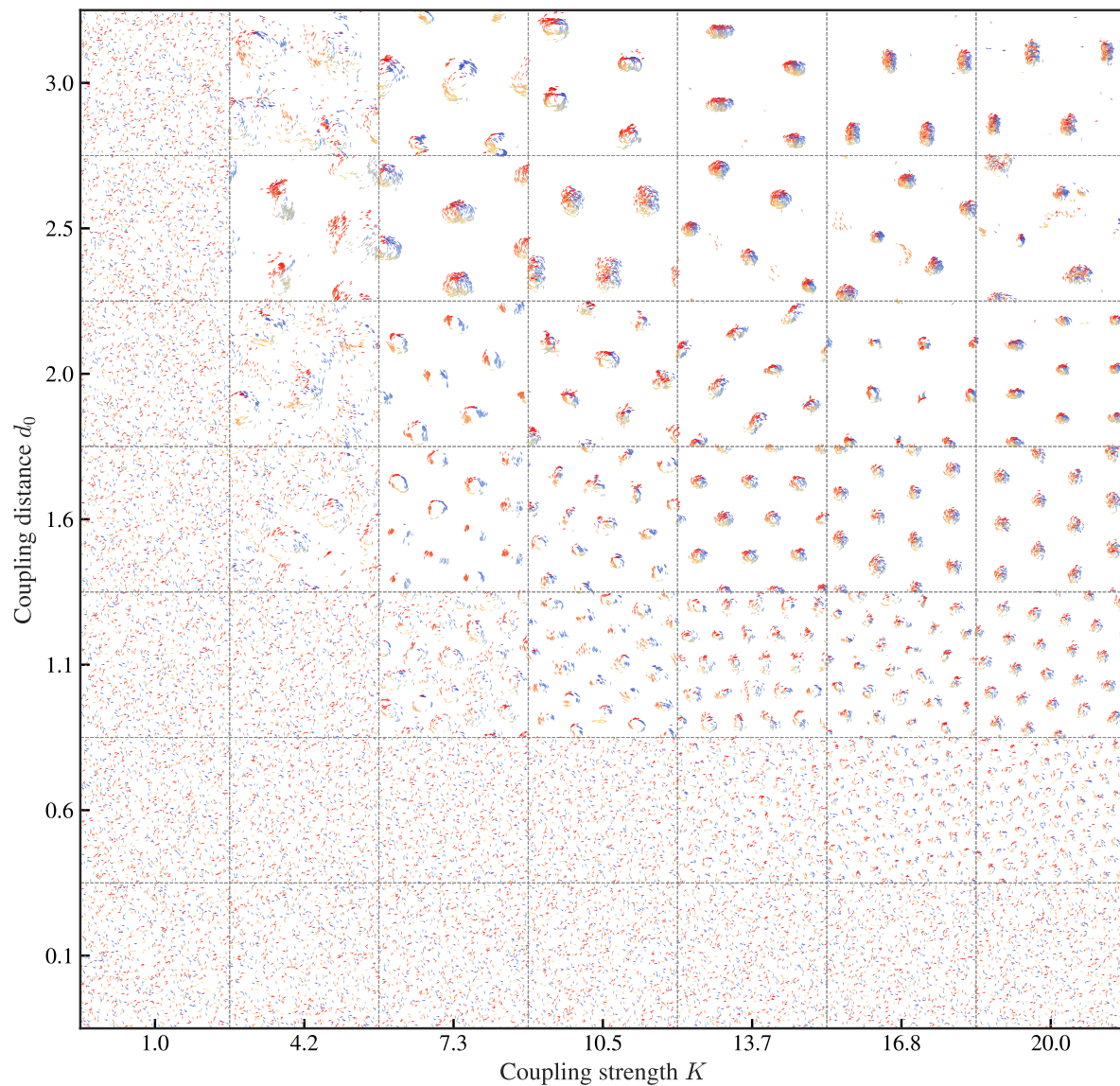


Figure 5: Snapshots of achiral system ( $\omega_{\min} = 0$  and  $\Delta\omega = 0$ ) at different coupling strengths  $K$  and radius  $d_0$  for  $\alpha = 0.6\pi$ .

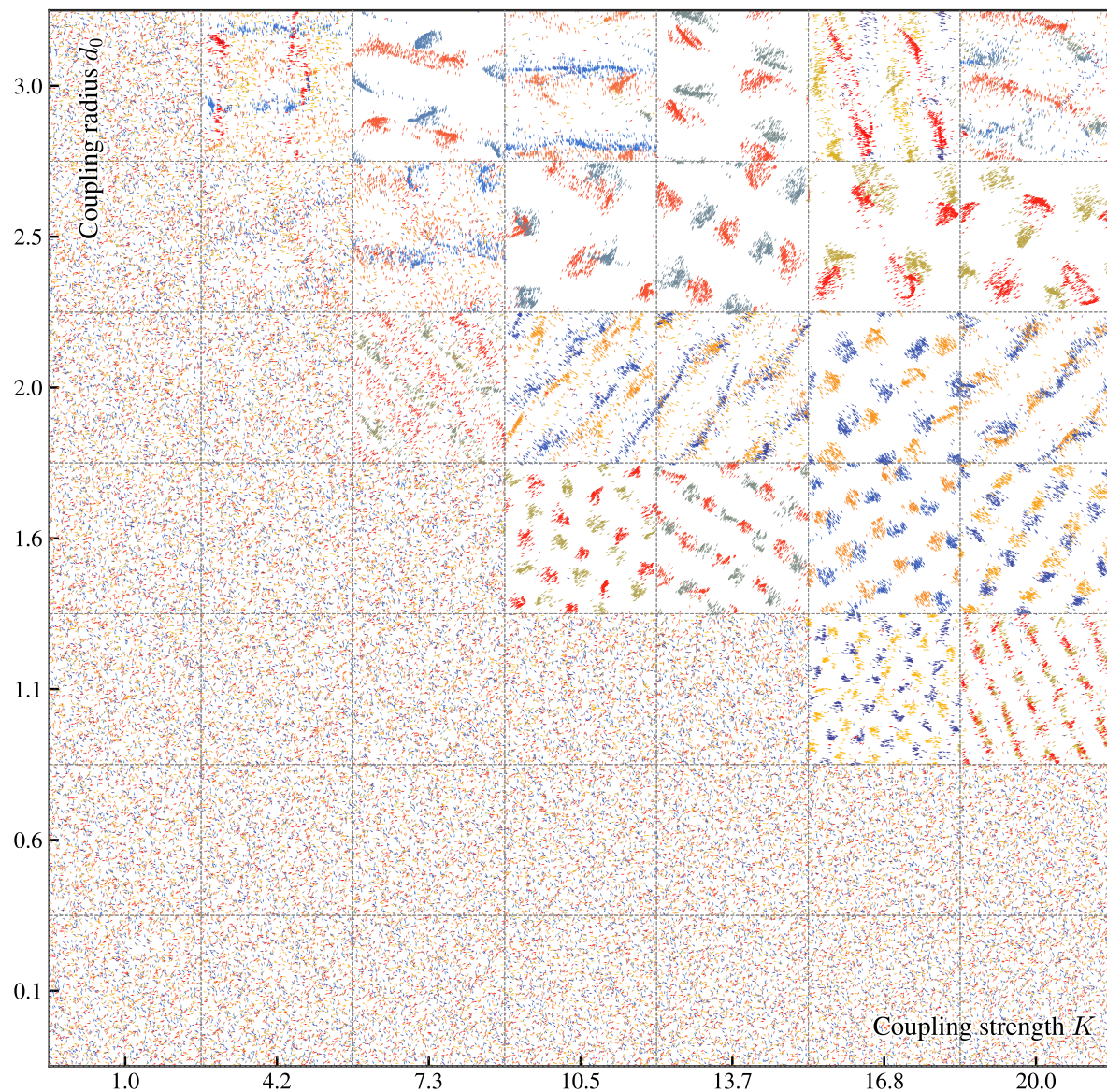


Figure 6: Snapshots of achiral system ( $\omega_{\min} = 0$  and  $\Delta\omega = 0$ ) at different coupling strengths  $K$  and radius  $d_0$  for  $\alpha = \pi$ .

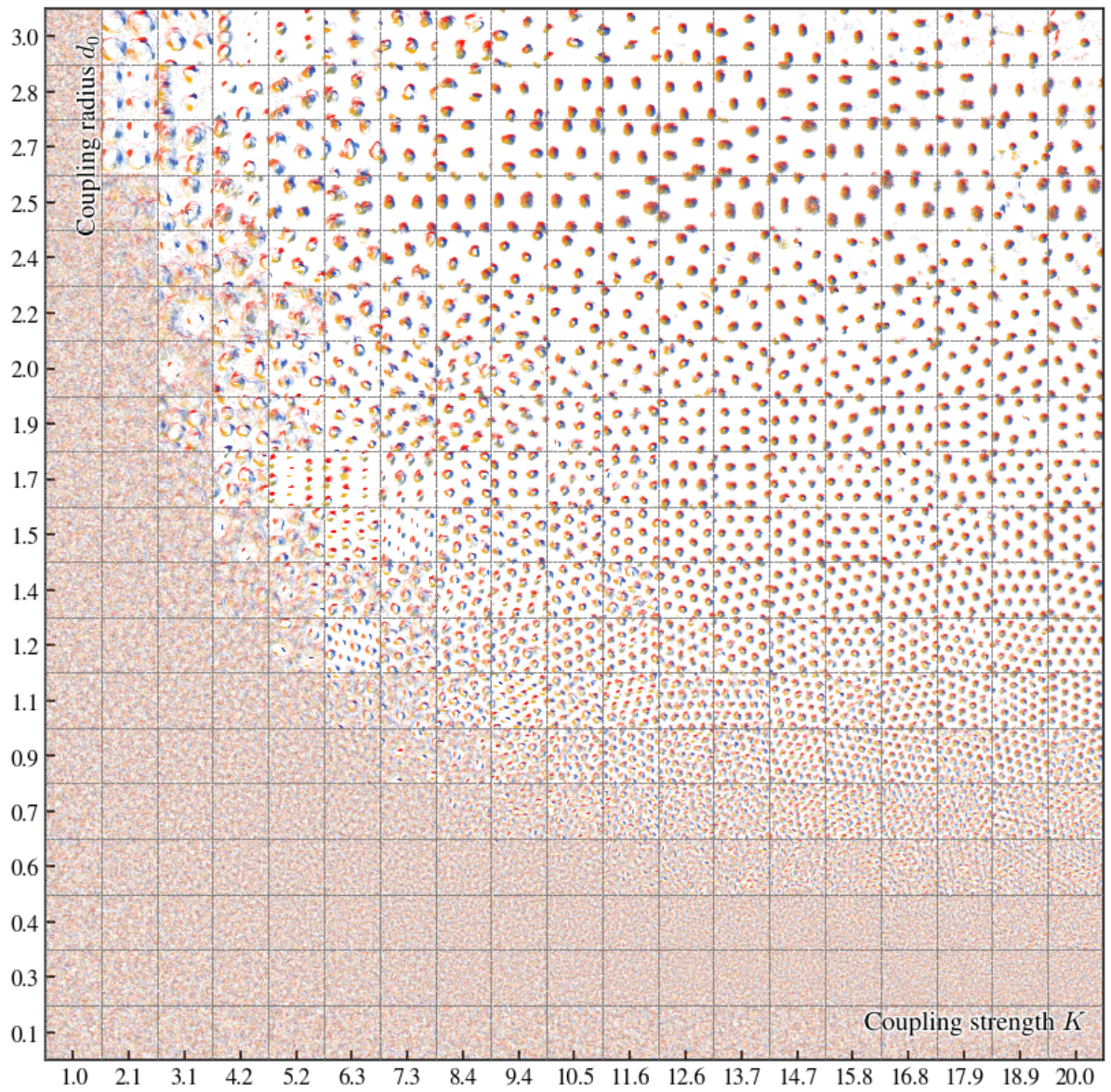


Figure 7: Snapshots of achiral system ( $\omega_{\min} = 0$  and  $\Delta\omega = 0$ ) at different coupling strengths  $K$  and radius  $d_0$  for  $\alpha = 0.6\pi$  with higher granularity.

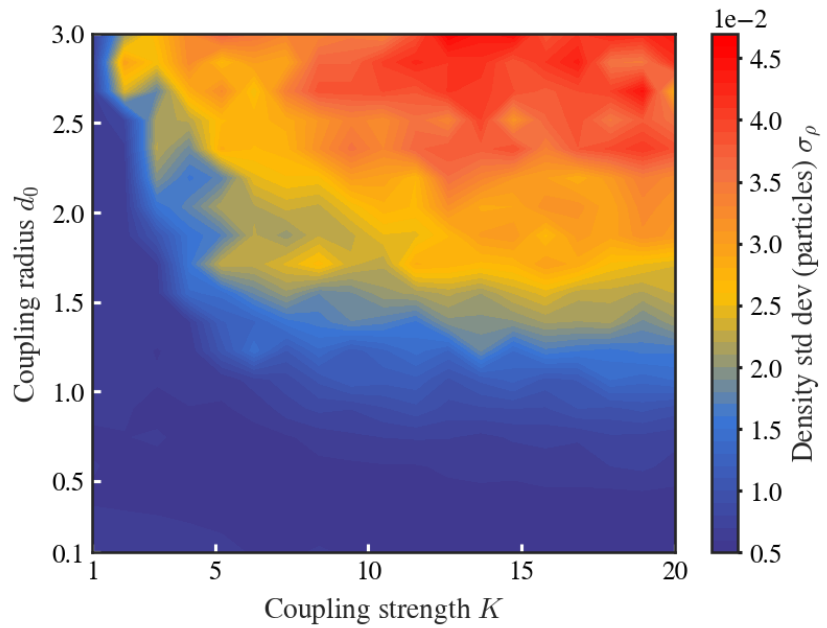


Figure 8: The order parameter  $\sigma_\rho(t)$  as a function of coupling strength  $K$  and radius  $d_0$  (Corresponding to Fig. 7). The color indicates the value of the order parameter.

### 2.1.2 Respiration-like motion of unit cells

For  $\alpha = 0.6\pi$ , the system exhibits the respiration-like motion of the cells. Since the phases of particles in each cell are uniformly distributed in  $[0, 2\pi]$  and the distance between cells is large enough to be considered decoupled, the effective frequency of each particle can be approximated by

$$\dot{\theta}_i = -K \sin \alpha + \frac{K}{|A_i|} \int_0^{2\pi} d\theta' \sin(\theta' - \theta_i + \alpha) = -K \sin \alpha , \quad (6)$$

and the lattice constant  $a$  can be approximated as

$$a = d_0 + 2 \frac{v}{K |\sin \alpha|} . \quad (7)$$

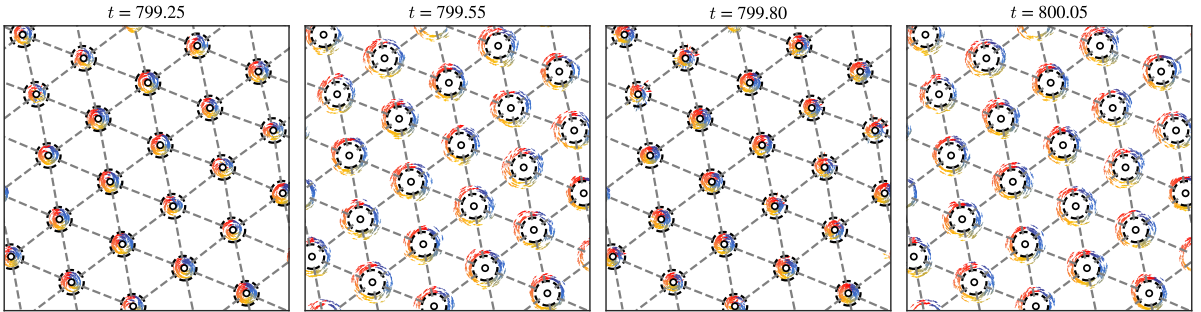


Figure 9: respiration-like motion of the cells with  $\omega_{\min} = 0$ ,  $\Delta\omega = 0$ ,  $N = 3000$ ,  $K = 10.5$ ,  $d_0 = 1.07$ , and  $\alpha = 0.6\pi$ . Black hollow dots represent the center of mass of each cell, black dash circles represent the theoretical unit cell radius  $v/\dot{\theta}_i$ , and the gray dash lines represent the theoretical distance between unit cells  $d_0$ .

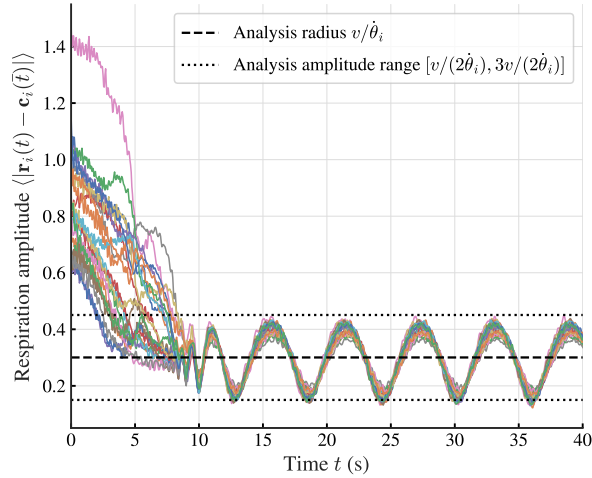


Figure 10: respiration amplitude of the system. The parameters are the same as in Fig. 9. Different colors represent different cells, and the amplitude is defined as the distance between particles and the center of mass of the cell at final state ( $\bar{t} = 40$ ).

As shown in Fig. 9 and Fig. 10, the respiration amplitude of the cells is defined as  $\langle |r_i(t) - c_i(\bar{t})| \rangle$ , where  $c_i(\bar{t})$  is the center of mass of the cell of  $i$ -th particle at final state ( $\bar{t} = 40$ ), and  $\langle \cdot \rangle$  denotes the average over all particles in the cell. It is worth noting that the amplitude is fluctuating around the theoretical cell radius  $v/\dot{\theta}_i$  and the respiration frequency of the cells exhibit synchronization.

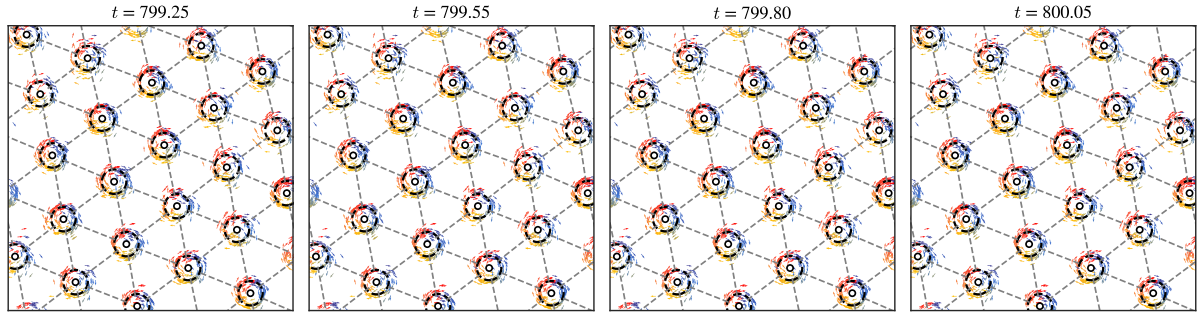


Figure 11: respiration-like motion of the decoupled cells. The parameters are the same as in Fig. 9.

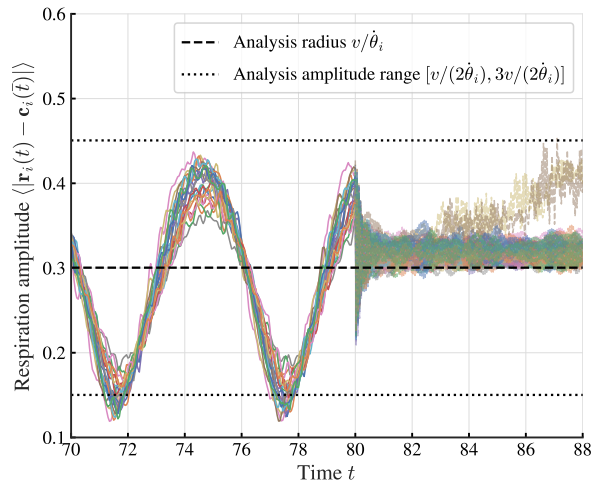


Figure 12: Respiration amplitude of the decoupled cells ( $t > 80$ ). The parameters are the same as in Fig. 9.

### 2.1.3 Lattice constant

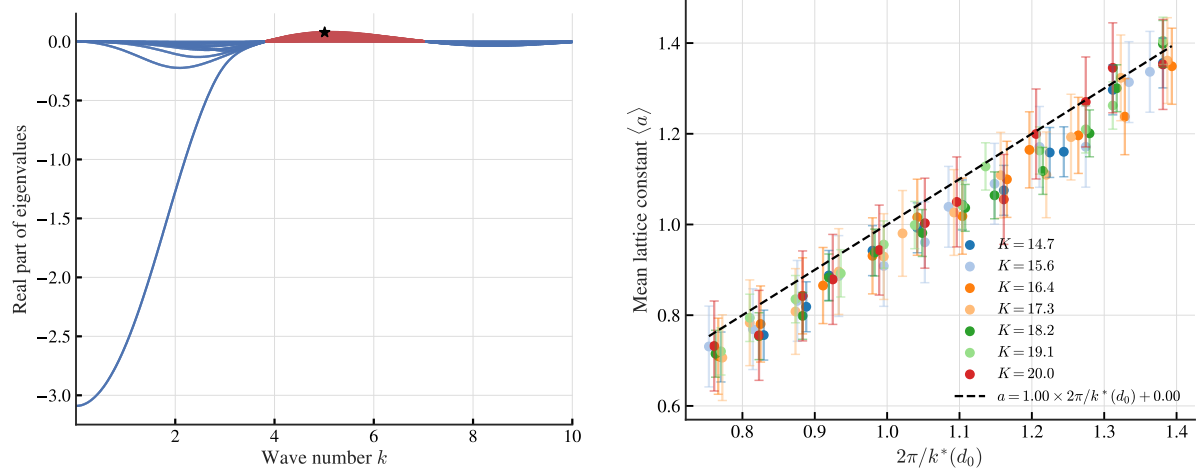


Figure 13: Lattice constant  $a$  as a function of coupling strength  $K$  and radius  $d_0$  for  $\alpha = 0.6\pi$ .

### 2.1.4 Initial conditions determined cells composition

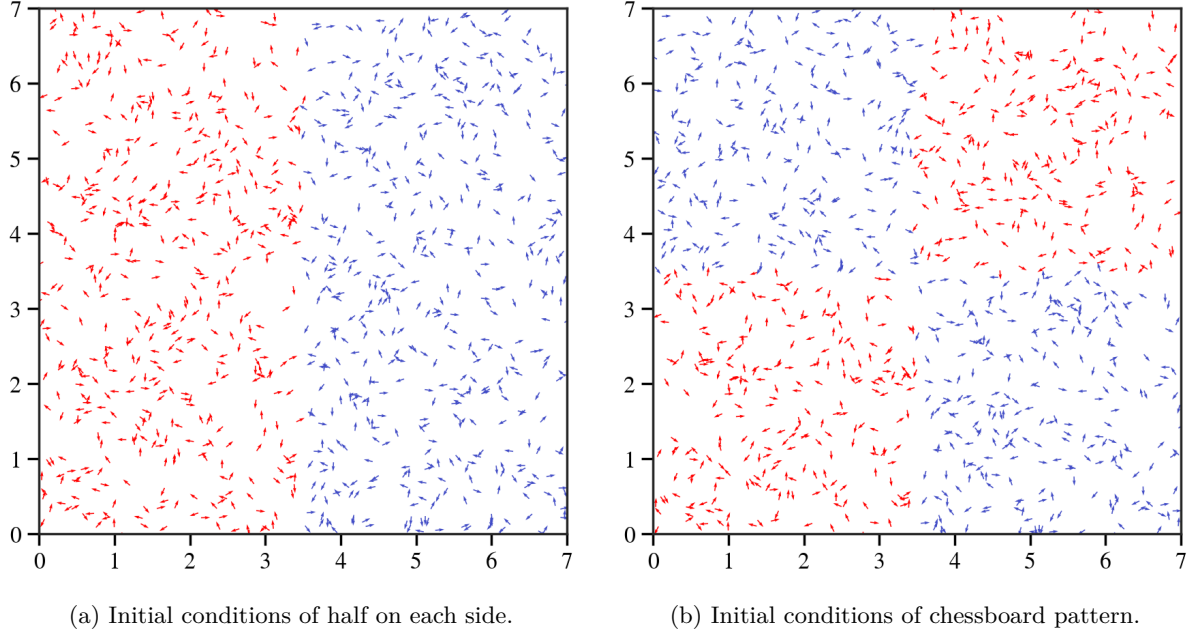


Figure 14: Two artificial non-uniform initial conditions in space. Red and blue particles represent particles with positive and negative chirality, respectively.

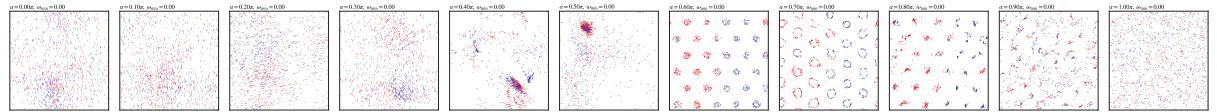


Figure 15: Snapshot of the system at  $t = 80$  with  $N = 1000$ ,  $K = 20$ ,  $\omega_{\min} = 0$ ,  $\Delta\omega = 1$  and initial conditions of half on each side.

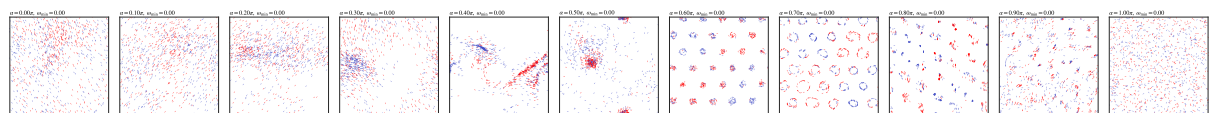


Figure 16: Snapshot of the system at  $t = 80$  with  $N = 1000$ ,  $K = 20$ ,  $\omega_{\min} = 0$ ,  $\Delta\omega = 1$  and initial conditions of chessboard pattern.

### 3 Critical condition for phase transition and mechanism

#### 3.1 Linear stability analysis with amplitude ansatz

In the thermodynamic limit  $N \rightarrow \infty$ , the state of the system in Eq. (1) can be characterized by the single-oscillator distribution  $\rho(\mathbf{r}, \theta, t)$ , which satisfies the continuity equation

$$\frac{\partial \rho}{\partial t} = -v \mathbf{p}(\theta) \cdot \nabla \rho - \frac{\partial}{\partial \theta} \{ \mathcal{T}[\rho] \rho \} , \quad (8)$$

where  $\mathcal{T}$  is the linear operator that has the form

$$\begin{aligned} \mathcal{T}[\rho] = & \frac{K}{A} \int_{L \times L} d^2 \mathbf{r}' \int_0^{2\pi} d\theta' \rho(\mathbf{r}', \theta', t) \\ & \times \Theta(d_0 - |\mathbf{r}' - \mathbf{r}|) [\sin(\theta' - \theta + \alpha) - \sin \alpha] , \end{aligned} \quad (9)$$

where  $\Theta(r)$  is Heaviside step function and

$$A = \int_{L \times L} d^2 \mathbf{r}' \int_0^{2\pi} d\theta' \rho(\mathbf{r}', \theta', t) \Theta(d_0 - |\mathbf{r}' - \mathbf{r}|) . \quad (10)$$

One obvious solution of Eq. (8) is  $\rho = (2\pi L^2)^{-1}$  representing a uniform disordered state. The stability of such a solution can be investigated by considering a small perturbation,

$$\rho(\mathbf{r}, \theta, t) = \frac{1}{2\pi L^2} + \varepsilon e^{\lambda(k)t+i\mathbf{k}\cdot\mathbf{r}} \Phi(\theta) , \quad (11)$$

with  $k = |\mathbf{k}| > 0$ , and linearizing the non-linear continuity equation (8), obtaining a eigenvalues problem to compute the  $\lambda(k)$  spectrum

$$(\mathcal{L}_0 - ivk\mathcal{L}_1) \Phi = \lambda \Phi , \quad (12)$$

$\mathcal{L}_0$  is diagonal in the basis  $\{e^{im\theta}\}_{m=-\infty}^{\infty}$ ,

$$\mathcal{L}_0 \Phi_m = \lambda_m^{[0]} e^{im\theta} , \quad (13)$$

with the eigenvalues

$$\lambda_m^{[0]}(k) = \frac{K J_1(kd_0)}{kd_0} (\delta_{m,-1} e^{i\alpha} + \delta_{m,1} e^{-i\alpha}) , \quad (14)$$

where  $J_1(x)$  is the Bessel function of the first kind of order one. The operator  $\mathcal{L}_1$  is defined as

$$\mathcal{L}_1 e^{im\theta} = \frac{1}{2} (e^{i(m+1)\theta-i\vartheta} + e^{i(m-1)\theta+i\vartheta}) , \quad (15)$$

where  $\vartheta$  is the forms  $\mathbf{k}$  with the  $x$  axis. Without the loss of generality, we can define the  $x$  axis parallel to  $\mathbf{k}$ , and, therefore, take  $\vartheta = 0$ .

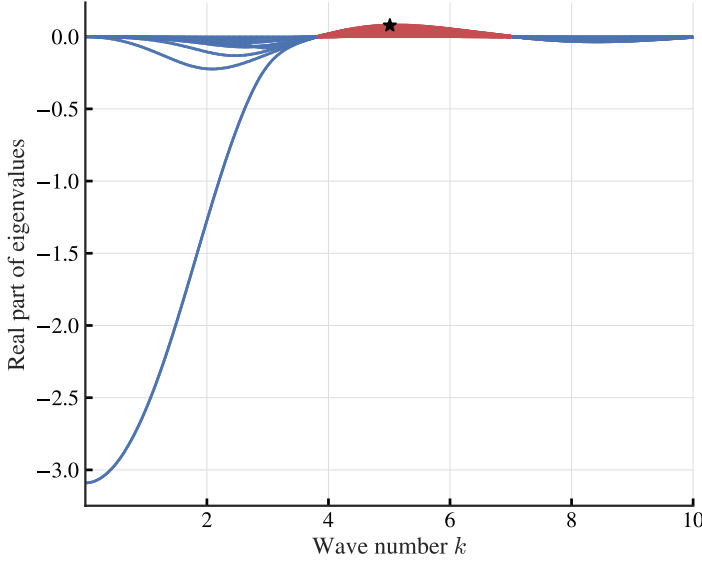


Figure 17: Continuous spectrum  $\text{Re}[\lambda_m^{[0]}(k)]$  as a function of wave number  $k$  for  $K = 20, d_0 = 1$ .

### 3.2 Abstract phase oscillator model

Let us consider a decoupled phase-oscillator system

$$\dot{\theta}_i = \omega_i - K \sin \alpha + \frac{K}{N} \sum_{j=1}^N \sin(\theta_j - \theta_i + \alpha) . \quad (16)$$

To quantify the phase coherence of the system, it is convenient to define the generalized complex-valued order parameters, i.e.,

$$Z(t) = R(t) e^{i\psi(t)} = \frac{1}{N} \sum_{j=1}^N e^{i\theta_j(t)}, \quad (17)$$

where  $n = 1, 2, \dots, N$ , and  $r(t)$ ,  $\psi(t)$  are the amplitudes and arguments of the order parameter. Our starting point is to analyze the critical point for the coherence of the order parameter. In the thermodynamic limit  $N \rightarrow \infty$ , the state of the system in Eq. (16) can be characterized by the single-oscillator distribution  $\rho(\theta, \omega, t)$ , which satisfies the continuity equation

$$\frac{\partial \rho}{\partial t} + \frac{\partial(\rho v)}{\partial \theta} = 0, \quad (18)$$

where  $\rho(\theta, \omega, t)$  accounts for the fraction of oscillators with phase  $\theta$  lying in the interval  $(\theta, \theta + d\theta)$  at fixed frequency  $\omega$  and time  $t$ , it satisfies the normalization condition

$$\int_0^{2\pi} \rho(\theta, \omega, t) d\theta = 1. \quad (19)$$

Here,  $v(\theta, \omega, t)$  is the velocity field, given by

$$v(\theta, \omega, t) = K \int_{-\infty}^{+\infty} \int_0^{2\pi} \sin(\theta' - \theta + \alpha) \rho d\theta' d\omega' + \omega - K \sin \alpha. \quad (20)$$

Correspondingly, the order parameter defined in Eq. (17) in the thermodynamic limit reads

$$Z(t) = \int_{-\infty}^{+\infty} g(\omega) d\omega \int_0^{2\pi} e^{i\theta} \rho(\theta, \omega, t) d\theta, \quad (21)$$

then  $v(\theta, \omega, t)$  simplifies to

$$v(\theta, \omega, t) = \omega - K \sin \alpha + \text{Im} [H(t) e^{-i\theta}] , \quad (22)$$

with the mean-field being

$$H(t) = KZ(t) e^{i\alpha} . \quad (23)$$

Since the distribution  $\rho(\theta, \omega, t)$  is  $2\pi$ -periodic in  $\theta$ , we can expand it in Fourier series as

$$\rho(\theta, \omega, t) = \frac{1}{2\pi} \sum_{n=-\infty}^{+\infty} a_n(\omega, t) e^{in\theta} , \quad (24)$$

where  $a_n(\omega, t)$  is the  $n$ -th Fourier coefficient. In particular, we have  $a_0(\omega, t) \equiv 1$  owing to the normalization condition in Eq. (19) and  $a_{-n}(\omega, t) = a_n^*(\omega, t)$ , where  $*$  denotes the complex conjugate.

According to the Ott-Antonsen ansatz [4, 5], it states that the  $n$ -th Fourier coefficient  $a_n(\omega, t)$  can be expressed in terms of the first-order coefficient, i.e.,  $a_n(\omega, t) = a^n(\omega, t)$ . In this regard, the evolution of  $\rho(\theta, \omega, t)$  degenerates to an invariant manifold, which is

$$\dot{a}(t) = i(K \sin \alpha - \omega) a(t) + \frac{1}{2} [H^*(t) - H(t) a^2(t)] . \quad (25)$$

Consequently, Eq. (25) is closed by the definition of the order parameter in Eq. (21), where

$$\begin{aligned} Z(t) &= \int_{-\infty}^{+\infty} g(\omega) a_{-1}(\omega, t) d\omega , \\ &= \int_{-\infty}^{+\infty} g(\omega) a^*(\omega, t) d\omega . \end{aligned} \quad (26)$$

We stress that Eq. (25) is still infinite dimensional because of the distributed natural frequencies. Thus, we may make a specific choice for the frequency distribution to get around this difficulty, e.g. a Lorentzian distribution  $g(\omega) = \Delta/[\pi(\omega - \mu)^2 + \Delta^2]$  with  $\Delta$  being the width of the distribution and  $\mu$  being the mean frequency. In this setting, the order parameters defined in Eq. (26) can be calculated by using Cauchy's residue theorem with analytical continuation of  $a(\omega, t)$  into the lower half complex plane, which leads to

$$Z(t) = a^*(\mu - i\Delta, t) . \quad (27)$$

As a result, the low-dimensional evolution of the order parameter can be obtained by replacing  $\omega$  with  $\mu - i\Delta$  and by taking into account the complex conjugate, which reads

$$\dot{Z} = -\Delta Z + iZ(\mu - K \sin \alpha) + \frac{1}{2} [KZe^{i\alpha} - KZ^*Z^2e^{-i\alpha}] . \quad (28)$$

Rewrite above equation using polar coordinates  $Z(t) = R(t) e^{i\psi(t)}$ , we have

$$\dot{R} = \frac{R}{2} (K - 2\Delta - KR^2) \cos \alpha , \quad (29a)$$

$$\dot{\psi} = \mu + \frac{K}{2} (R^2 - 1) \sin \alpha . \quad (29b)$$

Obviously, the amplitude  $R(t)$  is decoupled from the mean phase  $\psi(t)$  and Eq. (29a) have a critical coupling strength  $K_c = 2\Delta$  and a pair of critical phase frustration  $|\alpha_c| = \pi/2$ . Let us first consider the simplest case of  $\Delta = 0, \mu = 0$ , which corresponds to the case of achiral particles. In this case, when  $|\alpha_c| > \pi/2$ , the system bifurcates to  $R = 0$ , which corresponds to the incoherent state in phase oscillators and lattice state in self-propelled particles, while for  $|\alpha_c| < \pi/2$ , the system has a unique stable fixed point at  $R = 1$ , which corresponds to the coherent state and swarming state, respectively.

For the incoherent state, the system is totally disordered with the phases distributed uniformly around the unit circle, i.e.,  $\rho(\theta, \omega, t) = g(\omega)/2\pi$ , which implies that the phase velocity of each oscillator/particle becomes

$$\dot{\theta}_i = \omega_i - K \sin \alpha . \quad (30)$$

Correspondingly, the rotational radii of  $i$ -th particle is

$$r_i = \frac{v}{\dot{\theta}_i} = \frac{v}{\omega_i - K \sin \alpha} . \quad (31)$$

## References

- [1] Michel Fruchart, Ryo Hanai, Peter B. Littlewood, and Vincenzo Vitelli. Non-reciprocal phase transitions. *Nature*, 592(7854):363–369, Apr 2021.
- [2] D. Levis, I. Pagonabarraga, and B. Liebchen. Activity induced synchronization: Mutual flocking and chiral self-sorting. *Phys. Rev. Res.*, 1:023026, Sep 2019.
- [3] Benno Liebchen and Demian Levis. Collective behavior of chiral active matter: Pattern formation and enhanced flocking. *Phys. Rev. Lett.*, 119:058002, Aug 2017.
- [4] Edward Ott and Thomas M. Antonsen. Low dimensional behavior of large systems of globally coupled oscillators. *Chaos: An Interdisciplinary Journal of Nonlinear Science*, 18(3):037113, 09 2008.
- [5] Edward Ott and Thomas M. Antonsen. Long time evolution of phase oscillator systems. *Chaos: An Interdisciplinary Journal of Nonlinear Science*, 19(2):023117, 05 2009.
- [6] Hidetsugu Sakaguchi, Shigeru Shinomoto, and Yoshiki Kuramoto. Mutual entrainment in oscillator lattices with nonvariational type interaction. *Progress of Theoretical Physics*, 79(5):1069–1079, 05 1988.
- [7] Bruno Ventejou, Hugues Chaté, Raul Montagne, and Xia-qing Shi. Susceptibility of orientationally ordered active matter to chirality disorder. *Phys. Rev. Lett.*, 127:238001, Nov 2021.
- [8] Yujia Wang, Bruno Ventéjou, Hugues Chaté, and Xia-qing Shi. Condensation and synchronization in aligning chiral active matter. *Phys. Rev. Lett.*, 133:258302, Dec 2024.